RESEARCH ARTICLE
doi: 10.2306/scienceasia1513-1874.2026.013

ScienceAsia 52 (1): 2026: ID 2026013: **1–8**

Carboxyl-functionalized silica sphere-modified quartz crystal microbalance for ppb-level detection of aniline in water

Luyu Wang[a,*], **Jia Song**[b], **Chunyang Yu**[c]

[a] College of Artificial Intelligence and E-Commerce, Zhejiang Gongshang University Hangzhou College of Commerce, Hangzhou 311599 China
[b] School of Nuclear Science and Engineering, Shanghai Jiao Tong University, Shanghai 200240 China
[c] Design-AI Laboratory, China Academy of Art, Hangzhou 310009 China

[*]Corresponding author, e-mail: yucyzju@hotmail.com

Received 15 Nov 2024, Accepted 27 Jan 2026
Available online 21 Feb 2026

ABSTRACT: Aniline is one of the sources of water pollution and also a carcinogenic substance, posing a threat to ecological balance and human health. With the increasing demand for aniline detection, quartz crystal microbalance (QCM) detection is highly advantageous due to its high sensitivity and stable performance. Here, we fabricated carboxyl-functionalized silica spheres (SiO_2—COOH spheres) through a post-synthesis modification method. The SiO_2—COOH spheres were used as the sensing material in a QCM sensor for aniline detection in water. This QCM sensor could detect 10 ppb of aniline with a frequency shift of approximately 180 Hz within 150 s. Furthermore, the continuous response, selectivity, and anti-interference capability of the sensor were systematically investigated. This study shows that the method is fast and cost-effective and can be adapted to various on-site inspection sites.

KEYWORDS: sensor, quartz crystal microbalance, aniline, carboxyl functionalized silica spheres

INTRODUCTION

Aniline, an organic compound that exists as a colorless to pale yellow liquid, is widely used in industry as a pivotal raw material in the production of dyes, pesticides, rubber additives, pharmaceuticals, and numerous other products [1, 2]. However, its presence in water bodies poses significant risks [3]. Upon entering aquatic systems, aniline degrades water quality, which not only impedes the practical use of water resources but also poses potential threats to both aquatic life and human health [4]. When the concentration of aniline exceeds 100 ppm, exposure can have severe health impacts on organisms [5]. Additionally, aniline exhibits remarkable stability in the aquatic environment and resists degradation, thus posing a persistent threat to ecological habitats [6, 7]. Consequently, it is imperative to implement rigorous monitoring and control measures for aniline in water to safeguard environmental integrity.

The detection of aniline in water frequently relies on techniques such as gas chromatography, high-performance liquid chromatography, and spectrophotometry, among others. The detectable concentration range of these technologies for aniline is 0.6–3. ppm [8, 9]. While each of these methods possesses distinct advantages, they are commonly hampered by the drawbacks of being equipment-intensive and lacking portability. In contrast, sensors offer a unique balance between sensitivity and portability, thus emerging as an attractive alternative [10, 11]. Currently, fluorescence-based sensors are at the forefront of aniline detection in water, employing an array of innovative sensing materials such as graphene quantum dots, HOF-20, and Eu@UiO-66(COOH) [12–14]. These fluorescence sensors exhibit remarkable strengths in sensitivity, selectivity, and real-time monitoring capabilities. Nevertheless, their practical deployment necessitates the acknowledgment of inherent limitations, including potential interference, stringent illumination requirements, and intricate calibration procedures [15–18].

The quartz crystal microbalance (QCM) serves as an innovative sensing platform for the detection of harmful substances in water, featuring real-time stability, immunity to light interference, and broad versatility [19, 20]. Its operational principle revolves around converting the minute mass variations induced by the adsorption of target analytes onto the quartz crystal's surface into measurable shifts in the crystal's resonant frequency [21]. This transformation enables precise quantification of the analyte's mass through frequency measurements [22]. Accordingly, QCM has garnered widespread adoption across diverse domains, including gas analysis, viral detection, and heavy metal ion monitoring [23–25]. Nevertheless, despite such advancements, there remains a paucity of reports detailing QCM-based platform solutions specifically designed for the rapid and efficient detection of aniline in water.

Functionalized silica spheres are specific sensing materials, endowed with different detection characteristics through functionalization modification or adjustment of pore structure [26–28]. This research focuses on the development of a QCM sensor integrated with carboxyl-functionalized silica spheres (SiO_2—COOH spheres) for aniline detection in aquatic systems, as illustrated in Fig. 1. By adopting a post-synthesis mod-

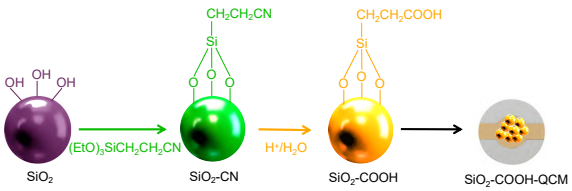

Fig. 1 Schematic diagram of the synthesis of SiO_2—COOH spheres and their modified QCM sensor manufacturing.

ification strategy, the SiO_2—COOH spheres improve the sensor's sensitivity, enabling it to swiftly detect aniline at concentrations as low as 10 ppb. This advanced sensor distinguishes itself by its capacity for continuous monitoring, exceptional selectivity, and robustness against interference from various waterborne ions, thus conferring substantial advantages over existing methods.

MATERIALS AND METHODS

Chemicals

Ammonia (28%), ethanol (99%), KCl (99.5%), toluene (99.8%), and tetraethyl orthosilicate (TEOS, 98%) was obtained from Aladdin Reagent Company (Shanghai, China). 3-cyanopropyltriethoxysilane (99%) was purchased from Sigma-Aldrich (Shanghai, China).

Synthesis of SiO_2 spheres

Monodisperse SiO_2 microspheres were synthesized using a modified Stöber method in ethanol with ammonia solution as the catalyst [29]. The reaction was carried out at 35 °C in a 250 ml flask with mechanical stirring at 300 rpm. Solution I, containing KCl (0.0015 g), ethanol (38 ml), water (6 ml), and ammonia (3 ml), was added into the flask first, and then solution II, containing ethanol (58 ml) and TEOS (5.64 g), was continuously added into the flask using a syringe pump over 2 h. After further reaction for 15 h, the obtained microspheres were purified by centrifugation and washing with ethanol three times. Finally, the microspheres were dried under vacuum at ambient temperature.

Synthesis of carboxyl-functionalized SiO_2 spheres

CN-modified SiO_2 spheres was achieved by refluxing the activated SiO_2 with 3-cyanopropyltriethoxysilane in dry toluene under nitrogen for 48 h. Then, the CN-modified SiO_2 spheres were hydrolyzed by heating in 50% (v/v) aqueous sulfuric acid at 150 °C for 3 h. After cooling to room temperature, the solid was filtered off, washed with an excess of deionized water, and dried at 110 °C overnight. The dried particle is designated as carboxyl-functionalized SiO_2 (SiO_2—COOH spheres).

Characterization of carboxyl-functionalized SiO_2

The morphology of SiO_2—COOH spheres was observed by scanning electron microscope (SEM, ZEISS Sigma 300, Germany). Wide angle X-ray diffraction patterns of the materials were obtained on a Bruker D2 Phaser diffractometer (Germany) using Cu Kα radiation. FT-IR spectra of the sample were measured on an FTIR-8400s (Shimadzu, Japan) spectrometer in the transmission mode. Standard KBr technique was applied.

Fabrication and testing methods of the QCM sensor

The fabrication and characterization processes for the SiO_2—COOH sphere-based QCM sensor conform to methods reported earlier [30]. Utilizing the Sauerbrey equation ($\Delta F = -2.26 \times 10^{-6} f^2 \Delta m/A$), the QCM resonator's ($\Delta F$) frequency shift correlates with the mass increment on the silver electrode (Δm). The QCM crystal underwent a specific processing method to apply the newly synthesized substances to the silver electrode's surface. This involved dispersing the materials in water (1 mg/ml) after ultrasonic treatment onto a purified QCM electrode, followed by drying the sensor in an infrared container at 333 K for 4 h to evaporate the solvent. As depicted in Fig. S1, prior to detection, 200 µl of distilled water was introduced into the test cell to serve as the detecting medium. Following the stabilization of the frequency signal for a few minutes, 1 µl of aniline solution (2 ppm) was meticulously administered into the cell using a microinjector. After injection of the aforementioned solution, the aniline concentration in the test cell reached 10 ppb. After aniline injection, the sensor exhibited a reduction in frequency, attributed to its confinement within the sensing material on QCM's surface.

Gaussian calculations

Gaussian 09 software was used with a DFT method employing the hybrid B3LYP functional and the 6-311++G(d,p) basis set to optimize the geometries of the molecules [31]. The optimized molecular structures were confirmed to be minima on the potential energy surface by vibration frequency analysis. In order to simulate the adsorption method between the SiO_2—COOH spheres and the aniline, the adsorption enthalpy (ΔH) between aniline molecule and SiO_2—COOH spheres was calculated according to the following Eq. (1).

$$\Delta H_{SiO_2\text{–COOH–aniline}}\left(\frac{kJ}{mol}\right) = \Delta H_{SiO_2\text{–COOH–aniline}}\left(\frac{kJ}{mol}\right) - \Delta H_{aniline} - \Delta H_{SiO_2\text{–COOH}}\left(\frac{kJ}{mol}\right) \quad (1)$$

RESULTS AND DISCUSSION

Material characterization

The microstructure of the samples was examined using scanning electron microscopy (SEM), with the results presented in Fig. 2. As depicted in Fig. 2a, the

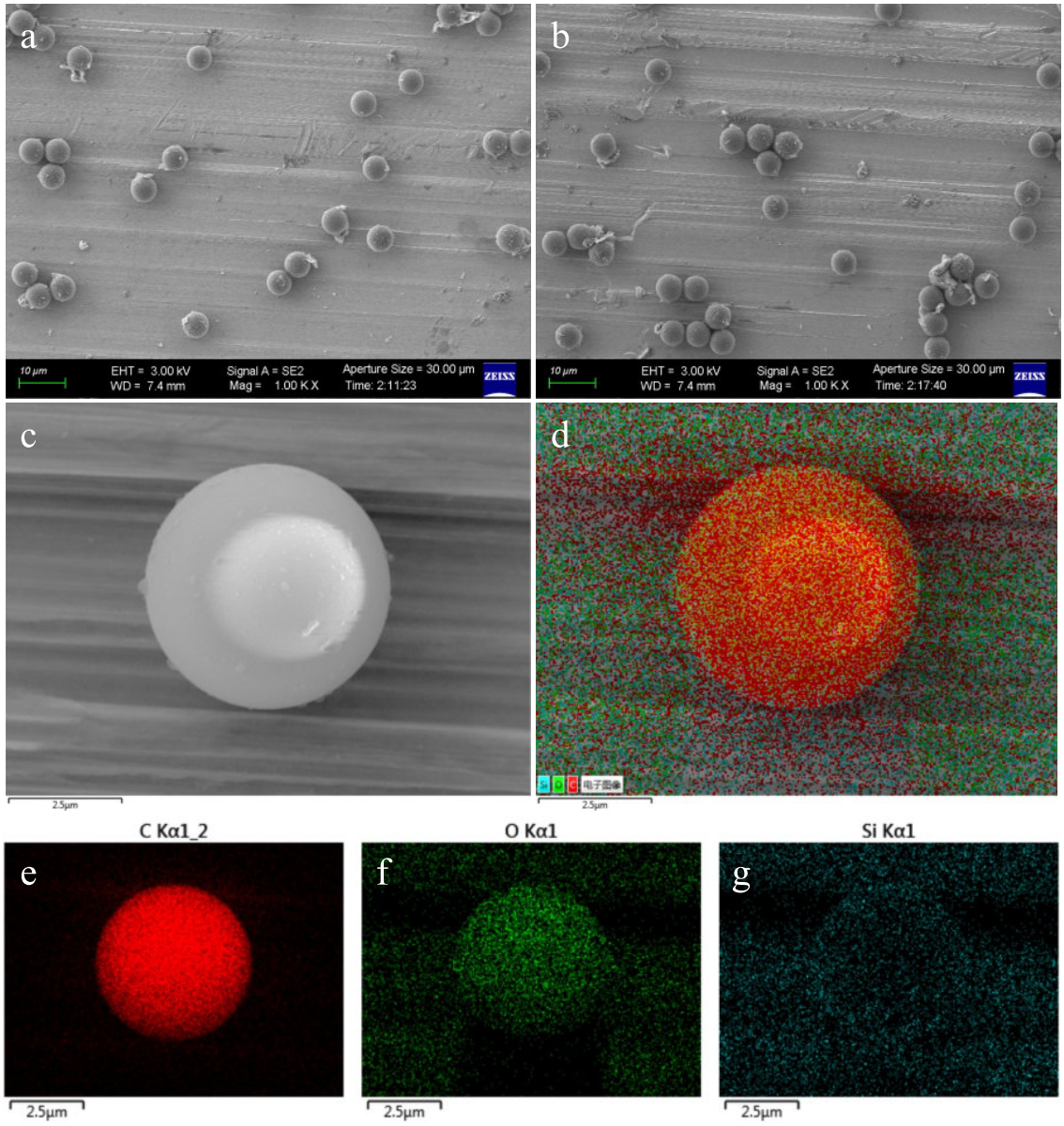

Fig. 2 SEM images of (a) SiO_2 spheres and (b) SiO_2—COOH spheres. (c)–(g) Scanning SEM image of SiO_2—COOH spheres with the corresponding elemental mapping of C, O, and Si.

SiO_2 spheres exhibit a uniform spherical morphology with a diameter of approximately 5 µm and a consistent distribution. Following carboxyl modification, the SiO_2—COOH spheres retain their spherical shape (Fig. 2b), exhibiting good particle dispersion and no significant agglomeration. This suggests that the introduction of —COOH functional groups did not alter the surface morphology of the SiO_2 spheres. Additionally, elemental mapping was conducted on SiO_2—COOH microspheres with superior morphology, as shown in Fig. 2c–g. Notably, besides the Si and O elements inherent to SiO_2, a uniformly distributed C element was also detected, which can be attributed to the —COOH functionalization.

The surface functional groups of SiO_2—COOH spheres were characterized via Fourier transform infrared (FTIR) spectroscopy. As shown in Fig. 3a, the bands observed at 805 cm^{-1} and 471 cm^{-1} correspond to the symmetric stretching of siloxane groups (Si—O—Si). Additionally, the prominent band at 1106 cm^{-1} is attributed to the asymmetric stretching of Si—O—Si [32]. Furthermore, the bands at 3432 cm^{-1}, 2933 cm^{-1}, and 1663 cm^{-1} are associated with O—H stretching vibration, asymmetric CH_2 vibration,

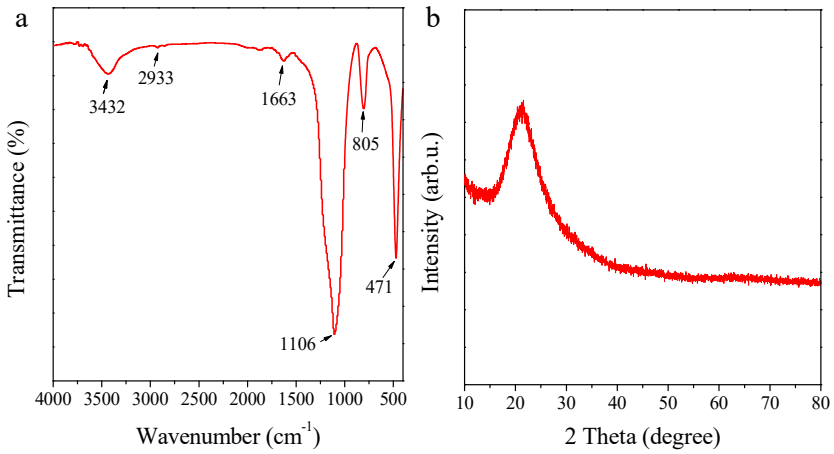

Fig. 3 (a) FT-IR spectra and (b) XRD pattern of SiO_2—COOH spheres.

and free COO— vibration, respectively [33]. These characteristic peaks confirm the successful grafting of —COOH groups onto the surface of the SiO_2 spheres. In Fig. 3b, the XRD pattern of SiO_2—COOH spheres exhibits similar characteristics of a broad amorphous peak, with no other notable peaks present, indicating their amorphous structure [34].

Aniline detection properties

An investigation was conducted to assess the sensitivity of SiO_2 and SiO_2—COOH spheres towards aniline in aqueous environments. As illustrated in Fig. 4a, SiO_2—COOH spheres exhibit a significantly higher frequency shift to various concentrations of aniline (ranging from 10 ppb to 60 ppb) compared to SiO_2 spheres. Furthermore, SiO_2—COOH spheres demonstrate over four times the responsiveness to aniline in water compared to SiO_2 spheres. This enhanced performance is attributed to the carboxyl groups present on the SiO_2—COOH spheres, which promote the adsorption of aniline molecules through hydrogen bonding interaction. This underscores the potential of SiO_2—COOH spheres as a superior sensing material for detecting aniline in water. Consequently, we opted to further evaluate the aniline detection capabilities of SiO_2—COOH spheres in a more comprehensive manner.

Fig. 4b presents a comparative analysis of the response frequency shifts observed between a pristine QCM sensor and a sensor coated with SiO_2—COOH spheres. The pristine QCM sensor, upon exposure to 10 ppb of aniline in water, exhibited a modest response frequency shift of approximately 8 Hz. Conversely, the SiO_2—COOH sphere-based sensor demonstrated a remarkable increase in response frequency shift, reaching 182 Hz under identical conditions. This striking disparity underscores the exceptional capacity of the SiO_2—COOH spheres to adsorb a significantly larger number of aniline molecules from the aqueous solution, thereby enhancing the sensitivity and overall performance of the sensor.

Fig. 5a meticulously portrays the shift in response frequency exhibited by the SiO_2—COOH sphere-based QCM sensor upon exposure to a range of aniline concentrations in water, spanning from 10 to 60 ppb, achieved through a series of injections of various aniline concentrations. As evident from Fig. 5a, the detection process for aniline was swiftly accomplished within 80 s for each 10 ppb concentration increment. The sensor sequentially encountered the aniline samples, with each incremental exposure lasting 220 s, prompting a consistent linear decline in the sensor's frequency signal. To further elucidate this correlation, Fig. 5b offers a dot-line plot derived from Fig. 5a, which underscores a clear and distinct linear relationship within the aniline concentration range of 10 to 60 ppb. The linear fitting equation derived is $y = -17.05x + 2.067$, where y signifies the frequency shift value and x represents the concentration of aniline in water. Notably, the coefficient of determination (R^2) is 0.9956, a value close to 1, thus confirming the high reliability of this fitting equation. To calculate the limit of detection (LOD) of this sensor, the formula LOD $= 3\sigma/S$ should be followed [35], where S represents sensitivity and σ represents the standard deviation of the calculated blank measurement. According to the linear fitting equation, the absolute value of the slope represents the sensitivity, which is $S = 17.05$ Hz/ppb. We tested 8 sets of blank samples, with measured values of −3.6, −4.1, −3.2, −3.8, −3.3, −4.0, −3.2, and −3.8 Hz, respectively. The calculated standard deviation σ was 0.3596. LOD $= 3\sigma/S = 0.063$ ppb.

To evaluate the selectivity of the SiO_2—COOH sphere-based QCM sensor, we conducted a comprehensive analysis of its response to various metal ions in water, specifically Cu^{2+}, Zn^{2+}, Fe^{3+}, K^+, and Na^+, each present at a concentration of 10 ppb. Fig. 6a illustrates the detection results, which indicate that the SiO_2—COOH sphere-based QCM sensor exhibits

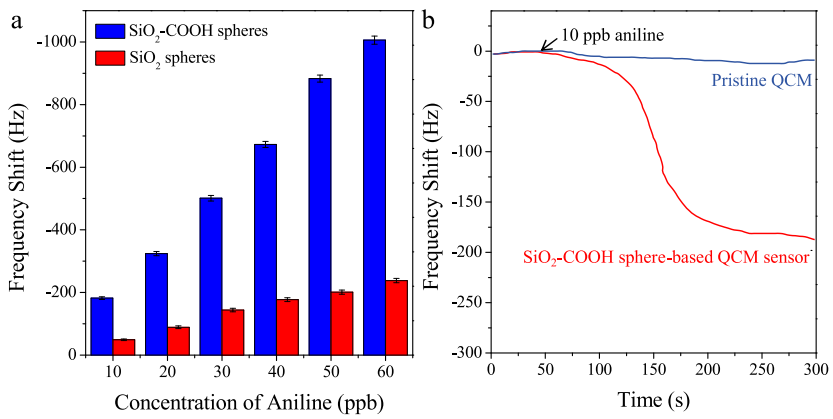

Fig. 4 (a) The frequency shift of SiO_2 and SiO_2—COOH spheres in response to aniline in water at different concentrations. (b) Response frequency shifts of the pristine QCM sensor and the SiO_2—COOH sphere-based sensor measured upon exposure to 10 ppb of aniline in water.

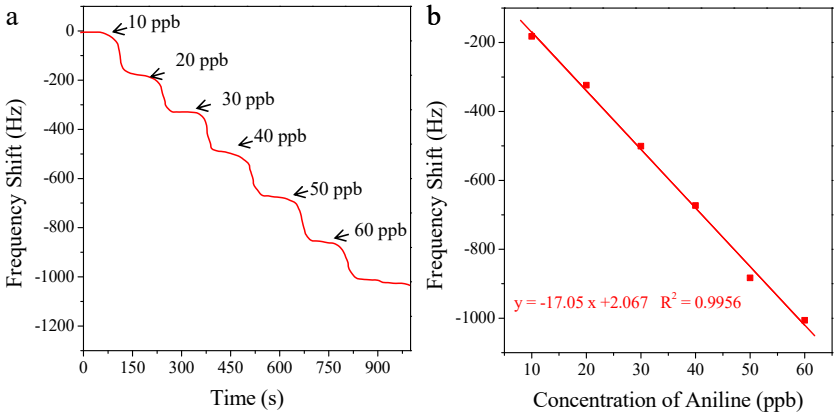

Fig. 5 (a) SiO_2—COOH sphere-based QCM sensor exhibiting a response frequency shift when exposed to varying concentrations of aniline in water, ranging from 10 to 60 ppb. (b) A pronounced linear relationship observed between the response frequency shift of the SiO_2—COOH sphere-based QCM sensor and the concentration of aniline dissolved in water. Specifically, in this context, the variable y is utilized to represent the frequency shift value, whereas x stands for the concentration of aniline present in the water.

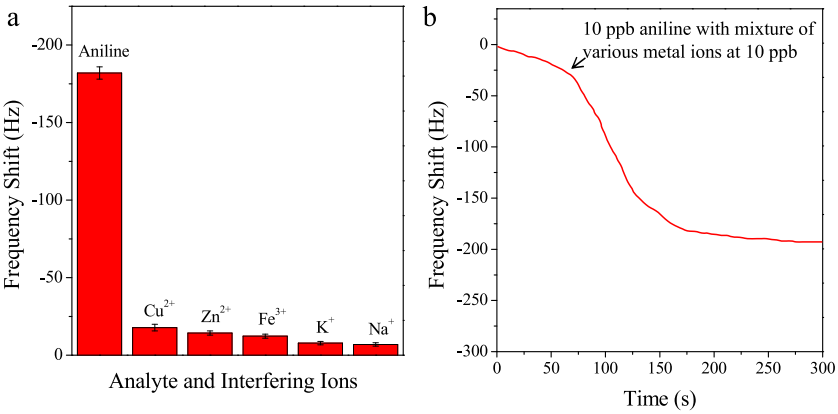

Fig. 6 (a) SiO_2—COOH sphere-based QCM sensor displaying distinct patterns of response frequency shifts when exposed to various metal ions at a concentration of 10 ppb. (b) Patterns of the response frequency shift for SiO_2—COOH sphere-based QCM sensor to a mixed solution containing aniline (10 ppb) in the presence of various metal ions (10 ppb).

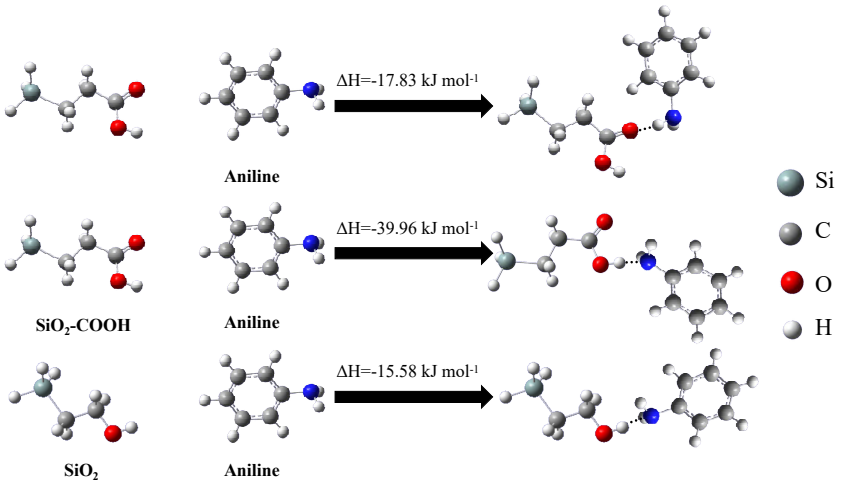

Fig. 7 Optimized geometries and interactions between the aniline molecule and the carboxyl group of SiO_2—COOH, as well as SiO_2.

a remarkable specificity for aniline in water, demonstrated by a substantial response frequency shift of 182 Hz. In stark contrast, the other ions tested only elicited negligible changes in the sensor's response. This result highlights the unique and high selectivity of the SiO_2—COOH sphere-based QCM sensor for aniline. The affinity of SiO_2—COOH spheres for aniline should originate from two weak adsorption interactions: hydrogen bonding adsorption between carbonyl oxygen atom and hydrogen atom of aniline, as well as adsorption between carbonyl hydrogen atom and nitrogen atom of aniline [36, 37]. To delve deeper into the influence of coexisting ions on aniline detection, we extended our investigation to a mixture solution containing Cu^{2+}, Zn^{2+}, Fe^{3+}, K^+, and Na^+ ions, each maintained at a concentration of 10 ppb. As depicted in Fig. 6b, the SiO_2—COOH sphere-based QCM sensor demonstrated a consistent response frequency shift of approximately 180 Hz. This robust performance signifies that aniline is preferentially adsorbed onto the SiO_2—COOH spheres, thereby enabling the sensor to accurately detect aniline in water with minimal interference from other ions present in the aqueous environment.

Sensing mechanism

The detection mechanism of the QCM platform relies on the adsorptive interaction between the sensing material and the target analyte [38]. To delve into the adsorption mode between SiO_2—COOH spheres and aniline, we employed Gaussian 09 software for simulation purposes. Initially, it is conceivable that hydrogen bonding may arise between the oxygen atom of the carboxyl group and the hydrogen atom of aniline. Furthermore, the hydroxyl moiety of the carboxyl group can engage in hydrogen bonding with the ammonia atom of aniline [36]. Gaussian 09 software was utilized to simulate the thermodynamic parameters associated with these two adsorption processes. Fig. 7 illustrates the enthalpy changes (ΔH) for these interactions, which are recorded as −17.83 kJ/mol and −39.96 kJ/mol, respectively. According to established adsorption theories, reversible physical adsorption is characterized by ΔH values ranging from −40 to 0 kJ/mol. Conversely, strong chemical reactions are indicative of ΔH values less than −80 kJ/mol. Weak chemical adsorption falls within the ΔH range of −80 to −40 kJ/mol [39]. Based on our simulation results, upon contact with the SiO_2—COOH sphere surface, aniline molecules interact with the carboxyl groups. Notably, this interaction with the carboxyl group is categorized as physical adsorption. Besides, the simulated ΔH for the adsorption of aniline onto SiO_2 (usually containing hydroxyl groups) was −15.58 kJ/mol (Fig. 7). This value is less negative than those for SiO_2—COOH, confirming the necessity of carboxylation for effective aniline adsorption.

CONCLUSION

In this study, we introduce a novel sensing material, carboxyl-functionalized SiO_2 spheres (SiO_2—COOH spheres), designed for the detection of aniline in aqueous environments using a QCM system. This sensor operates at low temperature and exhibits high sensitivity, with a detection limit as low as 10 ppb. Compared to pristine SiO_2 spheres, carboxyl functionalization significantly enhances the aniline-sensing performance of the SiO_2—COOH spheres. The superior sensing performance of the proposed sensor is attributed to the formation of hydrogen bonds between the carboxyl groups on the sphere surface and aniline molecules. This novel SiO_2—COOH material shows great application potential for aniline detection in aqueous systems.

Supporting information

The chemical raw materials and synthesis method of SiO_2—COOH spheres; characterization of carboxyl-functionalized SiO_2; fabrication and testing methods of the QCM sensor; Gaussian calculations; schematic diagram of the sensing evaluation system.

Appendix A. Supplementary data

Supplementary data associated with this article can be found at https://dx.doi.org/10.2306/scienceasia1513-1874.2026.013.

Acknowledgements: This research was supported by National Natural Science Foundation of China under Grant No. 62001420, Zhejiang Provincial Natural Science Foundation of China under Grant No. LQ21F010017, University-Industry Collaborative Education Program under Grant No. 220400576262052, and Science Foundation of Zhejiang Gongshang University Hangzhou College of Commerce, Zhejiang Gongshang University, China (ZJHZCC) under Grant No. 2222111.

REFERENCES

1. Seymour E, Lawrence N, Beckett E, Davis J, Compton R (2002) Electrochemical detection of aniline: an electrochemically initiated reaction pathway. *Talanta* **57**, 233–242.
2. Ghosh S, Malloum A, Bornman C, Othmani A, Osagie C, Esfahani Z, Khanday W, Ahmadi S, et al (2022) Novel green adsorbents for removal of aniline from industrial effluents: A review. *J Mol Liq* **345**, 118167.
3. Chen Y, Wang B, Wang X, Xie L, Li J, Xie Y, Li J (2019) A copper (ii)-paddlewheel metal-organic framework with exceptional hydrolytic stability and selective adsorption and detection ability of aniline in water. *ACS Appl Mater Interfaces* **9**, 27027–27035.
4. Bakier YM, Ghali M, Elkun A, Beltagi AM, Zahra WK (2021) Static interaction between colloidal carbon nanodots and aniline: A novel platform for ultrasensitive detection of aniline in aqueous media. *Mater Res Bull* **134**, 111119.
5. Chaturvedi NK (2022) Comparison of available treatment techniques for hazardous aniline-based organic contaminants. *Appl Water Sci* **12**, 173.
6. Nobrega MM, Temperini ML, Bini R (2017) Probing the chemical stability of aniline under high pressure. *J Phys Chem C* **121**, 7495–7501.
7. Luo J, Miao S, Koju R, Joshi T, Liu R, Liu H, Qu J (2022) Simultaneous removal of aromatic pollutants and nitrate at high concentrations by hypersaline denitrification: Long-term continuous experiments investigation. *Water Res* **216**, 118292.
8. Dorgerloh U, Hofmann A, Riedel J, Becker R (2023) Comparison of gas-and liquid chromatography-mass spectrometry for trace analysis of anilines in groundwater. *Int J Environ Anal Chem* **103**, 8465–8477.
9. Wu H, Du LM (2007) Spectrophotometric determination of anilines based on charge-transfer reaction. *Spectrochim Acta A Mol Biomol Spectrosc* **67**, 976–979.
10. Jiang Y, Sima Y, Liu L, Zhou C, Shi S, Wan K, Chen A, Tang N, et al (2024) Research progress on portable electrochemical sensors for detection of mycotoxins in food and environmental samples. *Chem Eng J* **485**, 149860.
11. Rasheed S, Kanwal T, Ahmad N, Fatima B, Najam-Ul-Haq M, Hussain D (2024) Advances and challenges in portable optical biosensors for onsite detection and point-of-care diagnostics. *Trends Anal Chem* **173**, 117640.
12. Gao X, Huang R, Fang W, Huang W, Yin Z, Liu Y, Huang X, Ding L, et al (2022) A portable fluorescence sensor with improved performance for aniline monitoring. *Adv Mater Interfaces* **9**, 2201275.
13. Wang B, He R, Xie L, Lin Z, Zhang X, Wang J, Huang H, Zhang Z, et al (2020) Microporous hydrogen-bonded organic framework for highly efficient turn-up fluorescent sensing of aniline. *J Am Chem Soc* **142**, 12478–12485.
14. Aly A, Ghali M, Osman A, El Nimr MK (2024) Non-synthetic luminescent graphene quantum dots in coconut water for aniline sensing applications. *Mater Res Bull* **171**, 112603.
15. Shin Y, Gutierrez-Wing MT, Choi J (2021) Recent progress in portable fluorescence sensors. *J Electrochem Soc* **168**, 17502.
16. Mccracken KE, Yoon J (2016) Recent approaches for optical smartphone sensing in resource-limited settings: A brief review. *Anal Methods* **8**, 6591–6601.
17. Würth C, Grabolle M, Pauli J, Spieles M, Resch-Genger U (2013) Relative and absolute determination of fluorescence quantum yields of transparent samples. *Nat Protoc* **8**, 1535–1550.
18. Putthithanad P, Rattanaumpa T, Pandhumas T, Budsombat S (2019) Sensitive 2, 4-dinitrotoluene fluorescence sensors based on porous electrospun fibres and porous membranes. *ScienceAsia* **45**, 36–42.
19. Erbahar DD, Gürol I, Gümüş G, Musluoglu E, Öztürk Z, Ahsen V, Harbeck M (2012) Pesticide sensing in water with phthalocyanine based qcm sensors. *Sens Actuators B Chem* **173**, 562–568.
20. Kushner DI, Hickner MA (2017) Water sorption in electron-beam evaporated SiO_2 on QCM crystals and its influence on polymer thin film hydration measurements. *Langmuir* **33**, 5261–5268.
21. Wang L, Song J, Yu C (2024) The utilization and advancement of quartz crystal microbalance (QCM): A mini review. *Microchem J* **199**, 109967.
22. Liu K, Zhang C (2021) Volatile organic compounds gas sensor based on quartz crystal microbalance for fruit freshness detection: A review. *Food Chem* **334**, 127615.
23. Fauzi F, Rianjanu A, Santoso I, Triyana K (2021) Gas and humidity sensing with quartz crystal microbalance (qcm) coated with graphene-based materials: A mini review. *Sens Actuators A Phys* **330**, 112837.
24. Navakul K, Sangma C, Yenchitsomanus P, Chunta S, Lieberzeit PA (2021) Enhancing sensitivity of qcm for dengue type 1 virus detection using graphene-based polymer composites. *Anal Bioanal Chem* **413**, 6191–6198.
25. Shaban A, Eddaif L (2021) Comparative study of a sensing platform via functionalized calix [4] resorcinarene ionophores on qcm resonator as sensing materials for detection of heavy metal ions in aqueous environments. *Electroanalysis* **33**, 336–346.
26. Zajc W, Czajkowski M, Cybiska J (2026) Forging insight: Unlocking the potential of silica spheres surface modification in sensing applications. *J Colloid Interface Sci* **704**, 139335.

27. Islam S, Bakhtiar H, Alshoaibi A, Haider Z, Riaz S, Naseem S (2020) Fast responsive thermally stable silica microspheres for sensing evaluation: sol-gel approach. *J Solgel Sci Technol* **96**, 614–626.
28. Petsong K, Luangchaisri C, Muangphat C (2025) Effect of mixing methods and chemical concentrations on the homogeneity of SiO_2 microsphere via Stöber and modified Stöber methods. *ScienceAsia* **51**, ID 2025017.
29. Lei X, Yu B, Cong H, Tian C, Wang Y, Wang Q, Liu C (2014) Synthesis of monodisperse silica microspheres by a modified Stöber method. *Integr Ferroelectr* **154**, 142–146.
30. Lou H, Zhang Y, Xiang Q, Xu J, Li H, Xu P, Li X (2012) The real-time detection of trace-level Hg^{2+} in water by qcm loaded with thiol-functionalized sba-15. *Sens Actuators B Chem* **166**, 246–252.
31. Yan D, Xu P, Xiang Q, Mou H, Xu J, Wen W, Li X, Zhang, Y (2016) Polydopamine nanotubes: bio-inspired synthesis, formaldehyde sensing properties and thermodynamic investigation. *J Mater Chem A Mater* **4**, 3487–3493.
32. Sharma P, Prakash J, Kaushal R (2024) Eco-friendly synthesis of amino and carboxyl-functionalized silica nanoparticles for enhanced adsorption of water pollutants. *Hybrid Adv* **6**, 100209.
33. Noma SAA, Ulu A, Koytepe S, Ate B (2020) Preparation and characterization of amino and carboxyl functionalized core-shell Fe_3O_4/SiO_2 for l-asparaginase immobilization: A comparison study. *Biocatal Biotransform* **38**, 392–404.
34. Zhang L, Song F, Wu Y, Cheng L, Qian J, Wang S, Chen Q, Li Y (2018) A novel amino and carboxyl functionalized mesoporous silica as an efficient adsorbent for nickel (ii). *J Chem Eng Data* **64**, 176–188.
35. Shao B, Ai Y, Yan L, Wang B, Huang Y, Zou Q, Fu H, Niu X, et al (2023) Wireless electrochemical sensor for the detection of phytoregulator indole-3-acetic acid using gold nanoparticles and three-dimensional reduced graphene oxide modified screen printed carbon electrode. *Talanta* **253**, 124030.
36. Wang L, Song J (2020) Enhanced nh3 sensing properties of carboxyl functionalized carbon nanocoil. *Mater Res Express* **7**, 75014.
37. Wang L, Wang B, Song J (2022) A carboxylated cellulose aerogel for the rapid detection of aniline vapor. *RSC Adv* **12**, 23169–23175.
38. Wang L, Gao J, Xu J (2019) QCM formaldehyde sensing materials: design and sensing mechanism. *Sens Actuators B Chem* **293**, 71–82.
39. Xu P, Yu H, Guo S, Li X (2014) Microgravimetric thermodynamic modeling for optimization of chemical sensing nanomaterials. *Anal Chem* **86**, 4178–4187.

Appendix A. Supplementary data

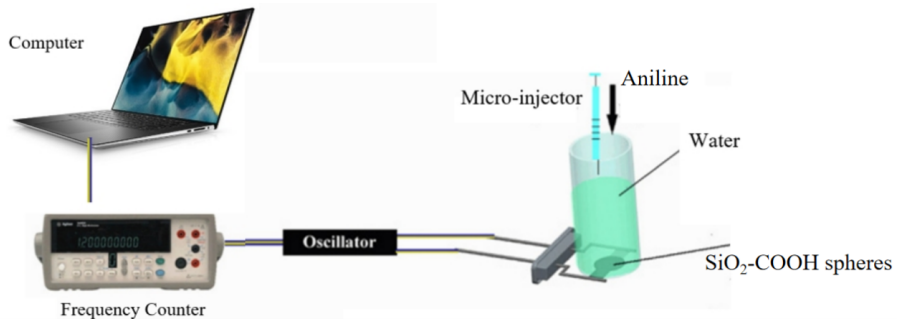

Fig. S1 Schematic diagram of the sensing evaluation system.